Journal of Solid State Chemistry **144,** 398–404 (1999)
Article ID jssc.1999.8178, available online at http://www.idealibrary.com on IDEAL®

Partial Oxygen Ordering in Cubic Perovskite $RE\mathrm{Ba_2Fe_3O_{8+w}}$ (RE = Gd, Eu, Sm, Nd)

J. Lindén,* P. Karen,† A. Kjekshus,† J. Miettinen,‡ and M. Karppinen§

*Department of Physics, Åbo Akademi, FIN-20500 Turku, Finland; †Department of Chemistry, University of Oslo, N-0315 Oslo, Norway; ‡Department of Technical Physics, Helsinki University of Technology, FIN-02015 Espoo, Finland; and §Laboratory of Inorganic and Analytical Chemistry, Helsinki University of Technology, FIN-02015 Espoo, Finland

Received August 18, 1998; accepted December 7, 1998

Single-phase samples of cubic $RE\mathrm{Ba_2Fe_3O_{8+w}}$ with RE = Gd, Eu, Sm, Nd were synthesized and equilibrated at 900°C in atmospheres with controlled partial pressures of oxygen. The oxygen content parameter w ranged from approximately -0.30, which is the lower decomposition limit, to between $w = 0.17$ for RE = Gd and $w = 0.37$ for RE = Nd, achieved in O_2 without crossing the upper limit. According to ^{57}Fe Mössbauer spectroscopy, all samples are antiferromagnets at room temperature, with iron in high-spin states ($S = 2$ for Fe^{2+} and Fe^{4+}; $S = 5/2$ for Fe^{3+}). The contents of divalent or, alternatively, tetravalent iron states are consistent with the stoichiometry of the samples. At the stoichiometric composition ($w = 0$), all Mössbauer components correspond to trivalent iron, differing only in the coordination geometries of their oxygen neighborhoods. The sum-up of the observed coordination numbers shows that the oxygen disorder in these cubic (by X-ray diffraction) phases is a linear combination of the two limiting cases of oxygen vacancy distribution: binomial (random) and ordered (one vacancy per every third pseudocubic cell). This corresponds to a gradual change from the long-range order seen in triple-perovskite-type phases (RE = Er to Dy) via a short-range order seen in the present systems (RE = Gd to Nd) to a fully random disorder (RE = La). Eventual variations in w affect the coordination statistics in details, but change the overall picture very little.

Key Words: **rare earth barium iron oxides; Mössbauer spectroscopy; perovskites oxygen ordering.**

I. INTRODUCTION

Long-range structural orderings in perovskite-type oxides that triplicate the (cubic) aristotype single cell are relatively rare. The importance of such orderings stems from the $RE\mathrm{Ba_2Cu_3O_{6+w}}$ superconducting oxides, but extends beyond that as this is one of the simplest orderings that supports two types of coordination polyhedra originating from the octahedral metallate network. The resulting charge transfers are of significance for a variety of cooperative phenomena as well as ionic and electronic transport properties, and these oxides represent good model systems.

In contrast to the mentioned cuprates that maintain the triplicate cell throughout nearly the entire rare-earth series, the ordering in $RE\mathrm{Ba_2Fe_3O_{8+w}}$ depends strongly on RE (1). Lanthanum easily blends with barium to yield a cubic structure, and only small rare earths, like Er, Dy, and Y, stabilize the triplicate cell. Their ordering with Ba occurs in synergy with the ordering of the six- and five-coordinated Fe atoms, which have ideally the same 1:2 ratio (when $w = 0$). Both powder neutron diffraction (2) and Mössbauer spectroscopy (3) studies confirm these special statistics of the iron coordinations. In cubic $\mathrm{LaBa_2Fe_3O_{8+w}}$ (1) the structural distinction between these iron coordinations is absent, and only Mössbauer spectroscopy is able to show (4) that the statistics of the iron coordinations at the single site corresponds to the binomial distribution of the oxygen vacancies [for all w; note that the oxygen vacancies do not order even when $w = 0$ (1)].

Also $RE\mathrm{Ba_2Fe_3O_{8+w}}$ phases with intermediately sized RE ions like Gd, Eu, Sm, and Nd are cubic according to powder diffraction, although the resulting Bragg reflections are somewhat broadened owing to the disorder-induced strain. The saturated oxygen contents of these phases follow a smooth curve between values typical for triple-perovskite-type $RE\mathrm{Ba_2Fe_3O_{8+w}}$ ($w \approx 0.1$ for RE = Dy) and the single cubic variants ($w \approx 0.8$ for RE = La) (1). In this study, Mössbauer spectroscopy is employed to establish whether the statistics of the iron coordinations at the crystallographically inseparable iron sites (as seen by powder diffraction) follow an abrupt structural change as a function of RE or show a tendency to the triplicate structural ordering.

II. EXPERIMENTAL

Syntheses. The oxide samples were synthesized from nanoscale precursors obtained by liquid mixing in citrate melts (5). High-purity reagents were used: dry, annealed

0022-4596/99 $30.00

Nd_2O_3, Sm_2O_3, Eu_2O_3, and Gd_2O_3 (>99.9 %); dried barium carbonate (0.1% Sr, Merck); and iron lumps (99.95%, Koch–Light). After the rare-earth oxides had been dissolved in melted citric acid monohydrate (reagent grade, Fluka), a solution of iron in diluted HNO_3 (Baker, analyzed) was gradually added into the hot melt, followed by liberation of nitrous gases. After cooling below 100°C, a small amount of water was added and $BaCO_3$ was dissolved. The clear viscous melt, formed under subsequent heating, was dehydrated into a solid at 180°C and milled, and the resulting fine powder was slowly incinerated in a crucible over two days at 450°C. The thus obtained precursor was calcined at 1000°C for 16 h in a flow of oxygen, pressed into pellets, and fired twice for 100 h at 1100°C with intermediate rehomogenization. These samples served as the $RE\mathrm{Ba_2Fe_3O_{8+w}}$ master samples for the oxygen content control in the region of $w > 0$. The master samples for $w < 0$ were obtained by reduction and sintering (at 1040, 985, 970, and 942°C for RE = Nd, Eu, Sm, and Gd, respectively) in atmospheres with the mixing Ar/H_2 volume ratio of approximately 60, saturated to $p_{H_2O} = 0.020$ bar. This procedure shortened the subsequent equilibration times by eliminating the slow crossing over the stoichiometric composition with trivalent Fe, and it diminished the reoxidation rate of divalent Fe.

Oxygen content control. The oxygen content was controlled by equilibrating the samples at suitable temperatures under defined partial pressures of oxygen, followed by quenching. The quenching apparatus had a vertical tube-furnace with the gas atmosphere flowing from the top and a massive brass quenching flange of a conical inner shape filled with high-purity Ar (<1 ppm of both O_2 and H_2O). Partial pressures of oxygen above some $p_{O_2} = 10^{-4}$ bar were obtained by mixing oxygen, argon, and water vapor; lower values were controlled by high-temperature equilibria in argon, hydrogen, and water vapor. The latter was introduced from a 45 wt% solution of H_3PO_4 at room temperature, and the saturated partial pressure of $p_{H_2O} \approx 0.02$ bar was corrected for the actual temperature and concentration of the H_3PO_4 solution. The high-temperature composition of the gas was calculated from the dilution ratios and thermodynamic data (6, 7) for H_2O formation. The equilibrations which normally lasted 3 days were prolonged to 8 days for compositions close to $w = 0$. The rate of quenching corresponded to 5–10 s to the disappearance of the red glow.

Oxygen content analyses. Oxygen contents were determined cerimetrically. Powdered samples were digested under ultrasound at 50–60°C for some 5 min in mixtures of concentrated hydrochloric acid and water (1 : 1 by volume when $w < 0$; 3 : 1 when $w > 0$; a precise amount of Mohr's salt added in the latter case), sealed in glass ampoules under Ar. Titrations were performed at room temperature under Ar in phosphoric acid complexed solutions with ferroin as an indicator.

Powder X-ray diffraction. Guinier–Hägg cameras with $CuK\alpha_1$ radiation and Si as an internal standard were used. The photographs were scanned by an LS-18 film scanner with software for X-ray data treatment (8).

Mössbauer spectroscopy. The Mössbauer absorbers were prepared by mixing approximately 40 mg of the sample material with varnish and evenly distributing it on an aluminum foil. The absorber diameter was 13 mm. Room-temperature measurements in transmission geometry were performed with an Amersham $^{57}Co : Rh$ (20 mCi, January 1995) source. The spectra were recorded between October 1997 and July 1998. A linear velocity scale with a maximum of 15 mm/s was applied. Selected samples were also measured at 90 K to decrease the experimental line width and to obtain additional information on the intensity ratios. The spectra were fitted with the full Hamiltonian of combined electric and magnetic interactions. The following hyperfine parameters were derived from these fits: the internal magnetic field experienced by the Fe nucleus (B), the chemical isomer shift relative to α-Fe (δ), the quadrupole coupling constant (eQV_{zz}), the resonance line widths (Γ), and the relative intensities of the components (I). The following conditions and constraints were applied: (i) For each component a certain variation in the parameter B was allowed in order to simulate the effect of local distortions of the coordination polyhedra. A gaussian distribution was assumed and its width (ΔB) was introduced as a fit parameter, which in the actual fits was observed to vary (with some constraints as explained in the results section) between $\Delta B \approx 2$ T for the most reduced samples and 4.5 T for the most oxidized samples. (ii) The asymmetry parameter η and the angle θ between the direction of the magnetic and the electric quantization axes were omitted. (iii) All components were constrained to have equal line widths Γ. (iv) A small asymmetric quadrupole component, originating from traces of iron in the Be detector window and in the Al foil, was kept fixed during the fit. The latter impurity defect covers less than 2% of the spectral intensity obtained in the measurements. In room-temperature spectra of samples with high oxygen contents, weak paramagnetic features developed in the center of the spectrum. Therefore an additional paramagnetic component was introduced in such cases (see, e.g., the $w = 0.17$ spectrum of Fig. 5). The origin of this paramagnetic component is discussed in more detail in Ref. (3).

III. RESULTS AND DISCUSSION

A. Compositional and Structural Characterizations

According to X-ray diffraction, all synthesized samples were single phase, with a cubic structure of the disordered

perovskite type. The unit-cell parameter a of the samples that have been used for Mössbauer spectroscopy measurements is plotted in Fig. 1 as a function of the oxygen content. The curves reflect the increasing atomic size of Fe with decreasing oxidation state, interrupted by a maximum around $w = 0$ that corresponds to all iron in the trivalent state. Also in the $RE\mathrm{Ba_2Fe_3O_{8+w}}$ phases with $RE =$ Er, Dy, Y, such maxima are observed, however, only in the unit-cell parameter c. The feature behind this is apparently the requirement of the bond-valence conditions in the constrained orthogonal network where the pyramidal and octahedral iron coordinations are joined and where the Fe oxidation occurs in the former and reduction in the latter coordination sphere (9).

The range in which the oxygen contents could be varied in $RE\mathrm{Ba_2Fe_3O_{8+w}}$ (RE = Nd, Sm, Eu, Gd) is appreciable. The lower homogeneity limits of these phases at 900°C are around $w = -0.30$, and two-phase mixtures of $RE\mathrm{BaFe_2O_{5+w}}$ (tetragonal, doubled perovskite-type cell) and a RE-stabilized $\mathrm{BaFeO_{3-w}}$ (a cubic-perovskite type) appear when these limits are crossed. The upper homogeneity limits have not been exceeded in the present experiments, where the maximum oxygen contents refer to 900°C and O_2 atmosphere. The oxygen contents increase from Gd to Nd, in apparent correlation with the increasing size of the trivalent RE ion, and are also expected to increase further on oxygen saturation at lower temperatures. A graphical illustration of the syntheses' conditions is provided in Fig. 2, where the dependence between the oxygen content in the sample and the partial pressure of oxygen in the equilibration atmosphere is plotted. A simple point-defect model is adopted that assumes that $RE\mathrm{Ba_2Fe_3O_{8+w}}$ is an acceptor-doped $\mathrm{LaFeO_3}$, compensated by oxygen vacancies. Given the oxygen content ranges, oxygen interstitials are neglected and this leaves only two variables to fit the oxygen content isotherm. These two variables are equilibrium constants for

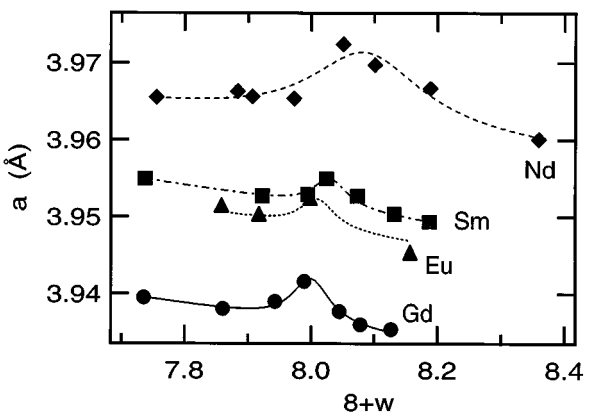

FIG. 1. Unit-cell parameter a for $RE\mathrm{Ba_2Fe_3O_{8+w}}$. Curves are fitted as guides for eye. Standard deviations do not exceed the size of the symbols.

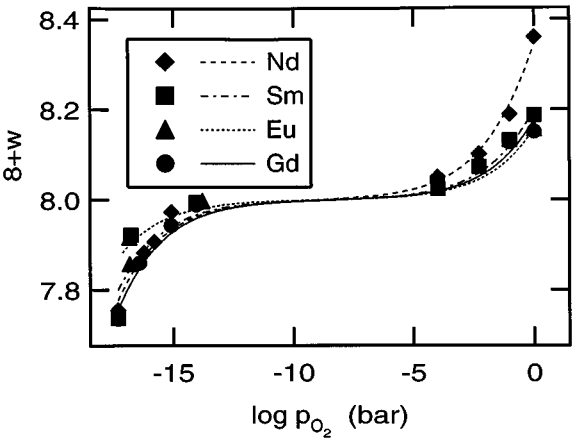

FIG. 2. Oxygen content versus partial pressure of oxygen for $RE\mathrm{Ba_2Fe_3O_{8+w}}$ quenched from 900°C. Standard deviations do not exceed the size of the symbols.

the following point-defect reactions:

$$\mathrm{O_2} + 2V_O^{\bullet\bullet} \rightleftharpoons 4h^{\bullet} + 2\mathrm{O}_O^{x} \qquad [1]$$

and

$$2\mathrm{O}_O^{x} \rightleftharpoons 4e' + 2V_O^{\bullet\bullet} + \mathrm{O_2}, \qquad [2]$$

which together describe the oxygen exchange. Combining the mass action terms with the electroneutrality condition $[e'] + [\mathrm{Ba}'_{\mathrm{La}}] = [h^{\bullet}] + 2[V_O^{\bullet\bullet}]$ gives (after expressing $[V_O^{\bullet\bullet}]$ in terms of w) a polynomial function of w and $\log p_{\mathrm{O_2}}$ whose numerical solution is fitted to the experimental data. Figure 2 illustrates that the conditions of the quenching are reasonably consistent in that no major violations of the expected trends occur.

Magnetic susceptibility measurements have been performed (by SQUID magnetometer; up to 300 K) and confirmed that the phases are antiferromagnetically (AF) ordered for all investigated compositions, having T_N well above the measurement range.

B. Mössbauer Spectroscopy

The Mössbauer spectra are typical of AF ordering in all measured samples of $RE\mathrm{Ba_2Fe_3O_{8+w}}$ with RE = Nd, Sm, Eu, Gd. A weak paramagnetic component is seen in the most oxidized samples. The dominant presence of the magnetic interactions facilitates a much more detailed resolution in terms of the coordination, valence, and spin states of Fe.

For direct comparisons with the ideal, ordered, triple-perovskite-type model, samples with $w \approx 0$ are best suited. Room-temperature spectra with fitted curves for such samples are shown in Fig. 3, based on component assignments

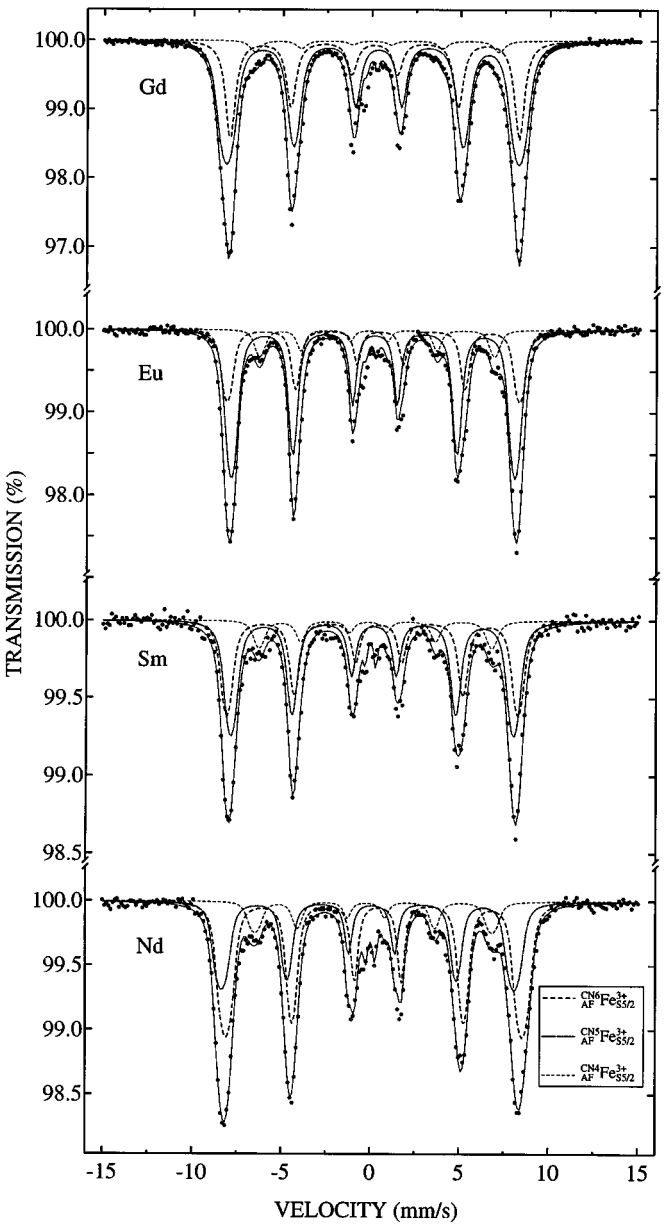

FIG. 3. Mössbauer spectra of $RE Ba_2Fe_3O_{8.00\pm0.01}$ at 296 K. Labeling of the components is shown at the bottom of the figure.

that are described in detail in Ref. (3). Three components are clearly discerned and correspond to the coordination numbers CN6, CN5, and CN4 for trivalent iron. These components are hence the same as identified in cubic $LaBa_2Fe_3O_{8+w}$. According to a binomial model (3) for distribution of oxygen vacancies (per one coordination octahedron, which is joined into a corner-sharing infinite network), theoretical intensities for $w = 0$ are 49% (CN6), 37% (CN5), 12% (CN4), and 2% (CN3). The ordered triple-perovskite model (4) has one oxygen vacancy at every third cubic pseudocell and hence 33% (CN6) and 67% (CN5) for the same ideal composition. The intensities actually obtained for these components are plotted as a function of the *RE* ionic radii in Fig. 4 and compared with the situation seen for RE = La and RE = Dy, which to a good approximation correspond to the two limiting oxygen-vacancy distributions. It is seen that, as a function of the *RE* ionic size, the participation of these two limiting distributions undergoes a gradual, practically linear change. Figure 4 clearly suggests that the transition from the cubic to the tetragonal structure is preceeded by a partial ordering of the oxygen atoms. This partial ordering is of the triple-perovskite type with two square pyramids apically connected to an octahedron, but occurs only on a short-range scale and is not resolved in X-ray diffraction patterns.

To gain additional information on the Mössbauer components, samples with a wide range of oxygen stoichiometry were measured. With spectra for selected RE = Gd samples like the examples in Fig. 5, the hyperfine parameters obtained from fittings of the full series of the RE = Gd spectra are presented in Table 1. (In fitting the room-temperature spectra, maximum ΔB values of 1.5 and 4.5 T were constrained for the $^{CN4}Fe^{3+}$ and $^{CN6}Fe^{3+}$ component, respectively, in order to prevent interferences.)

In addition to the components already considered for the stoichiometric samples ($w = 0$), two additional components were found for $w < 0$ and one for $w > 0$. On inspection of the values for the isomer shifts (see Ref. (3)) it was straightforward to identify them as divalent and tetravalent Fe for $w < 0$ and $w > 0$, respectively. The same components were identified also for RE = Nd, Sm, Eu. However, increasing

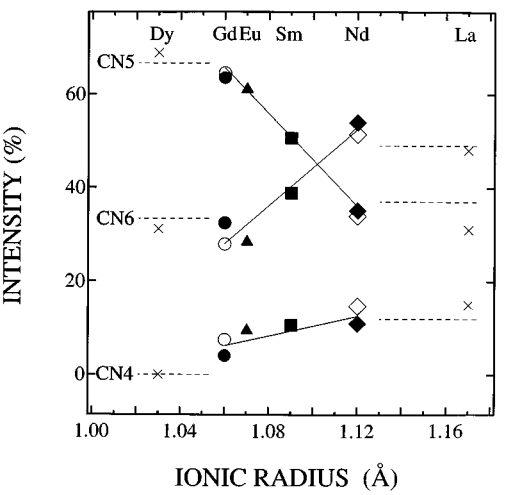

FIG. 4. Distribution of CNs in $RE Ba_2Fe_3O_{8.00\pm0.01}$ as a function of the Shannon–Prewitt (10) RE^{3+} radii in terms of intensities of Mössbauer components at 296 K (filled) and 90 K (open). Data for RE = Dy (4) and La (3) are taken to represent the two limiting distributions of oxygen vacancies.

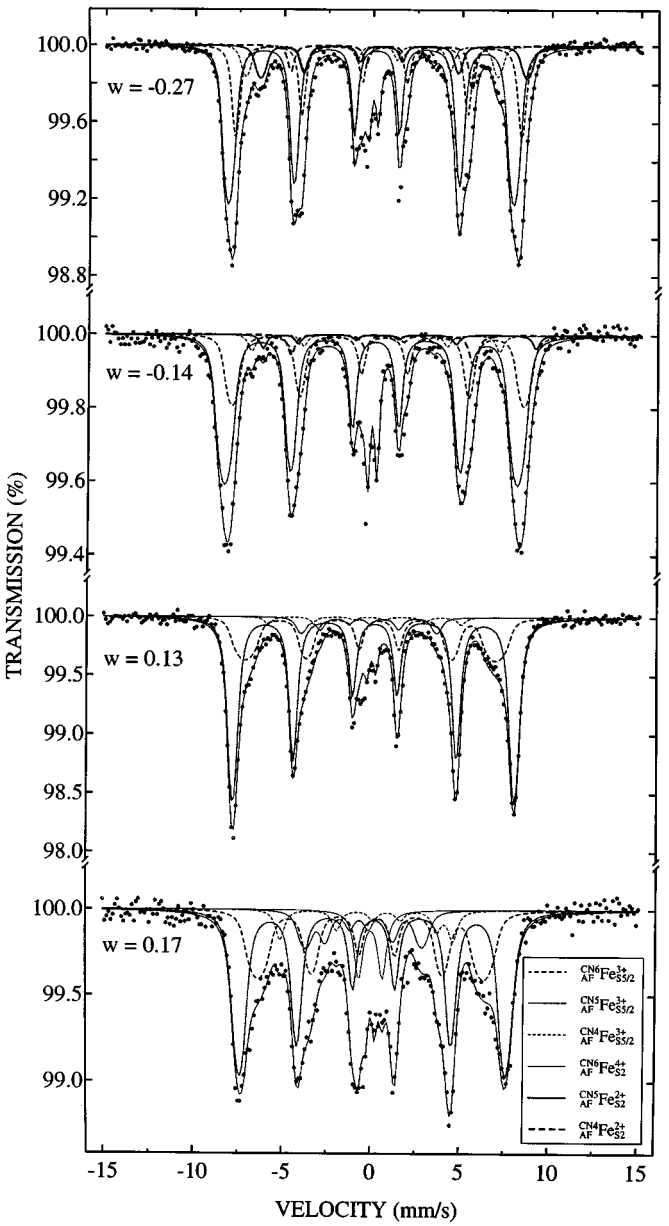

FIG. 5. Selected Mössbauer spectra of $GdBa_2Fe_3O_{8+w}$ at 296 K. Labeling of the components is shown at the bottom of the illustration. A paramagnetic component, present only in the $w = 0.17$ spectrum, is drawn with a thin full line.

oxygen disorder causes the Mössbauer lines to broaden, making it somewhat more difficult to discern the components, in particular for the Nd variant. The origin of the two divalent components is not obvious. The assumption that they reflect two different coordinations (the couples CN5 and CN4 or CN4 and CN3) is plausible by structural and bond-valence arguments. The $^{CN5}Fe^{2+}$ and $^{CN4}Fe^{2+}$ couple is judged as more likely and used in further considerations.

Among the valence, spin, coordination, and magnetic states, assigned from the four hyperfine Mössbauer parameters, there are two that relate directly to the composition of the sample. These are the coordination and valence states, and both can be used to verify the assignments through compositional accounting.

According to the approach via coordination, the oxygen content per $REBa_2Fe_3O_{8+w}$ formula corresponds to $3 \times CN/2$ (three single-perovskite cells per formula; each oxygen shared by two cells). Using intensities of the components for weighting, the assigned coordination numbers are converted into oxygen content, shown in Fig. 6 as a function of the actual composition. Note that only low-temperature Mössbauer data are used in Fig. 6. The reason is that these data have line widths sufficiently narrow to avoid interferences of the $^{CN4}_{AF}Fe^{3+}$ component with other components. (Such interferences are, e.g., manifested in an unreasonable increase of the intensity of $^{CN4}_{AF}Fe^{3+}$; see Table 1.)

When evaluating the agreement in Fig. 6, one must keep in mind that assumptions have been made during the CN assignments, for weak components in particular. As an example, CN for tetravalent Fe has been *assumed* to be six, and CN5/CN4 *chosen* for the two divalent components as discussed above. Considering these limitations, Fig. 6 shows that the assignments of the coordination numbers to the components are reasonable.

With component intensities again as the weighting factor, the valence states from the assigned components are converted into the average iron valence and plotted in Fig. 7 against the actual oxygen content parameter of the samples.

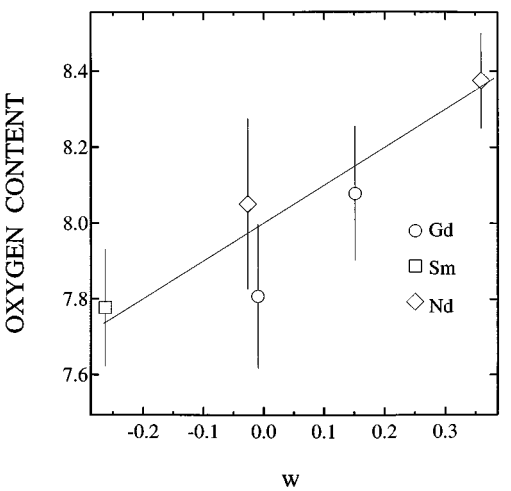

FIG. 6. Oxygen content in $REBa_2Fe_3O_{8+w}$ when calculated from the CN values extracted from components in Mössbauer spectra at 90 K. Error bars are marked. The solid line represents the correspondence between the two coordinates.

TABLE 1
Internal Magnetic Fields (B), Chemical Isomer Shifts (δ), Quadrupole Coupling Constants (eQV_{zz}) and Spectral Intensities (I) for AF Components[a] of Mössbauer Spectra of $GdBa_2Fe_3O_{8+w}$ at 296 K[b]

	w	${}^{CN6}_{AF}Fe^{3+}_{S5/2}$	${}^{CN5}_{AF}Fe^{3+}_{S5/2}$	${}^{CN4}_{AF}Fe^{3+}_{S5/2}$	${}^{CN4}_{AF}Fe^{2+}_{S2}$	${}^{CN5}_{AF}Fe^{2+}_{S2}$	${}^{CN6}_{AF}Fe^{4+}_{S2}$
B	− 0.27	49.74	49.62	43.84	46.3	31.6	
(T)	− 0.14	50.68	50.83	43.06	47.4	31.9	
	− 0.08	50.39	50.17	43.10	46.9	31.0	
	− 0.01	50.29	50.83	42.47			
	0.05	48.99	50.17	42.66			24.66
	0.08	49.16	49.85	42.30			23.48
	0.13	44.55	48.94	37.55			22.62
	0.15	44.07	48.56	36.72			23.10
	0.17	39.24	46.37	30.05			20.32
δ	− 0.27	0.565	0.146	0.154	0.88	1.56	
(mm/s)	− 0.14	0.606	0.172	0.284	1.00	1.68	
	− 0.08	0.554	0.166	− 0.095	1.08	1.20	
	− 0.01	0.254	0.239	0.317			
	0.05	0.299	0.297	0.384			− 0.313
	0.08	0.239	0.310	0.381			− 0.169
	0.13	0.326	0.286	0.387			− 0.318
	0.15	0.329	0.285	0.299			− 0.348
	0.17	0.318	0.284	0.465			− 0.388
eQV_{zz}	− 0.27	− 0.69	− 0.64	− 0.60	1.4	− 4.2	
(mm/s)	− 0.14	− 0.71	− 0.49	0.02	2.5	− 4.0	
	− 0.08	− 0.80	− 0.45	1.10	1.8	− 4.1	
	− 0.01	0.01	− 0.63	0.57			
	0.05	− 1.66	0.02	− 1.12			1.03
	0.08	− 1.52	0.07	− 1.06			1.42
	0.13	− 0.87	− 0.11	− 0.68			0.63
	0.15	− 0.77	− 0.09	− 1.03			0.59
	0.17	− 0.67	− 0.14	− 2.24			0.50
I	− 0.27	22.28	53.52	8.71	10.1	5.4	
(%)	− 0.14	26.18	62.69	3.81	2.82	4.48	
	− 0.08	29.05	59.77	4.68	3.62	2.87	
	− 0.01	32.41	63.54	4.05			
	0.05	23.92	68.40	4.53			3.15
	0.08	23.57	64.37	8.23			3.82
	0.13	29.70	60.46	4.31			5.53
	0.15	30.61	56.38	5.48			7.53
	0.17	30.12	51.58	6.84			11.5

[a]A weak paramagnetic component is observed in the most oxidized sample.
[b]Values for the Mössbauer parameters for RE = Eu, Sm, and Nd may be obtained from the first author.

The agreement supports the assignment of the valence states in the discerned Mössbauer components throughout the range in oxygen contents and for both room-temperature and 90 K data.

Accounting of the assigned valence states leads to a clearer agreement with the sample compositions. The reason is that three major components refer to the same valence state (Fe^{3+}), but different coordinations. The statistical errors of their intensities then roughly cancel when accounting in terms of valences is made and appear for accounting according to coordinations.

Having the assignments of the major Mössbauer components well ascertained, it is possible to conclude that the oxygen disorder in the stoichiometric $RE Ba_2Fe_3O_8$ phases ($w = 0$) with medium-sized RE atoms corresponds to a linear combination of two 'extreme' types of oxygen-vacancy distributions as a function of the RE ionic size: the binomial (random) distribution and the ordered (one vacancy every third pseudocubic cell) distribution. Although this gradual change from order to disorder appears as a rather sudden crossover from tetragonal to cubic symmetry in the powder diffraction patterns, it may manifest itself in an array of

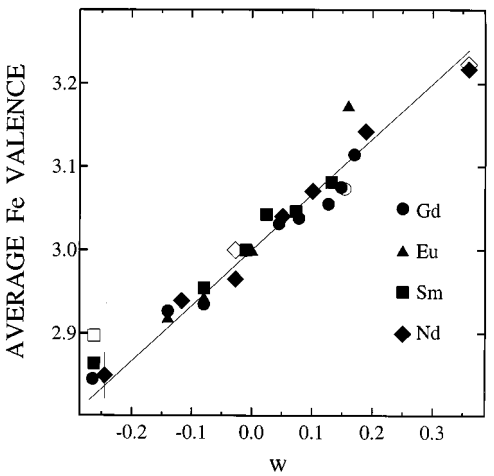

FIG. 7. Average Fe valence in $RE\mathrm{Ba_2Fe_3O_{8+w}}$, when calculated from the valence-state values extracted from components in Mössbauer spectra at room temperature (filled) and 90 K (open). The solid line represents the correspondence between the two coordinates. A typical standard deviation is indicated in the lower left corner.

order-sensitive cooperative phenomena and charge transport mechanisms. Variations in w across the homogeneity range add little to this general picture; only the statistics of the occurring coordinations is accordingly shifted.

ACKNOWLEDGMENT

Mr. T. Pietari from Helsinki University of Technology is thanked for performing some of the Mössbauer measurements.

REFERENCES

1. P. Karen, A. Kjekshus, Q. Huang, J. W. Lynn, N. Rosov, I. Natali-Sora, V. L. Karen, A. D. Mighell, and A. Santoro, *J. Solid State Chem.* **136,** 21 (1998).
2. Q. Huang, P. Karen, V. L. Karen, A. Kjekshus, J. W. Lynn, A. D. Mighell, N. Rosov, and A. Santoro, *Phys. Rev. B*: *Condens. Matter* **45,** 9611 (1992).
3. J. Lindén, M. Lippmaa, P. Karen, A. Kjekshus, and M.Karppinen, *J. Solid State Chem.* **138,** 87 (1998).
4. J. Lindén, A. Kjekshus, P. Karen, J. Miettinen, and M. Karppinen, *J. Solid State Chem.* **139,** 168 (1998).
5. P. Karen and A. Kjekshus, *J. Amer. Ceram. Soc.* **77,** 547 (1994).
6. I. Barin and O. Knacke, "Thermochemical Properties of Inorganic Substances," pp. 316 and 584. Springer, Berlin, 1973.
7. I. Barin, O. Knacke, and O. Kubashevski, "Thermochemical Properties of Inorganic Substances, Supplement," p. 295. Springer, Berlin, 1977.
8. P. E. Werner, "The Computer Programme SCANPI 9," Institute of Inorganic Chemistry, University of Stockholm, Sweden, 1992.
9. P. Karen, A. Kjekshus, Q. Huang, I. Natali-Sora, J. W. Lynn, N. Rosov, V. L. Karen, A. D. Mighell, and A. Santoro, in preparation.
10. R. D. Shannon and C. T. Prewitt, *Acta Crystallogr. Ser. B* **25,** 925 (1969).